NANO LETTERS

Letter

pubs.acs.org/NanoLett

Chemical Management for Colorful, Efficient, and Stable Inorganic–Organic Hybrid Nanostructured Solar Cells

Jun Hong Noh,[†] Sang Hyuk Im,[‡] Jin Hyuck Heo,[†] Tarak N. Mandal,[†] and Sang Il Seok*[,†,§]

[†]Division of Advanced Materials, Korea Research Institute of Chemical Technology, 141 Gajeong-Ro, Yuseong-Gu, Daejeon 305-600, Korea

[‡]Department of Chemical Engineering, College of Engineering, Kyung Hee University, 1 Seochon-dong, Giheung-gu, Youngin-si, Gyeonggi-do 446-701, Republic of Korea

[§]Department of Energy Science, Sungkyunkwan University, Suwon 440-746, Korea

S *Supporting Information*

ABSTRACT: Chemically tuned inorganic–organic hybrid materials, based on $CH_3NH_3(=MA)Pb(I_{1-x}Br_x)_3$ perovskites, have been studied using UV–vis absorption and X-ray diffraction patterns and applied to nanostructured solar cells. The band gap engineering brought about by the chemical management of $MAPb(I_{1-x}Br_x)_3$ perovskites can be controllably tuned to cover almost the entire visible spectrum, enabling the realization of colorful solar cells. We demonstrate highly efficient solar cells exhibiting 12.3% in a power conversion efficiency of under standard AM 1.5, for the most efficient device, as a result of tunable composition for the light harvester in conjunction with a mesoporous TiO_2 film and a hole conducting polymer. We believe that the works highlighted in this paper represent one step toward the realization of low-cost, high-efficiency, and long-term stability with colorful solar cells.

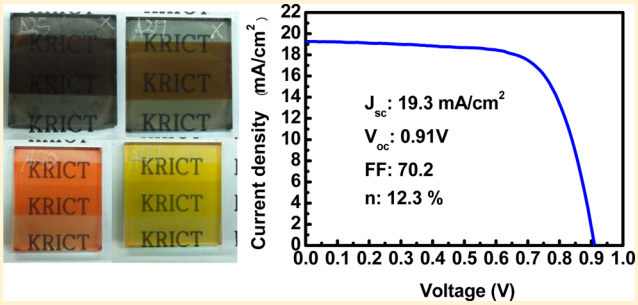

KEYWORDS: *Inorganic–organic hybrid, nanostructured, colorful, efficient and stable solar cells*

Solar energy is the largest noncarbon-based energy source. As opposed to more conventional resources such as coal and fossil fuels, solar energy can serve as a means to solving the serious issue of global warming that has arisen from the evolution of CO_2. The use of solar cells is an effective method of converting solar energy into electric energy, and it represents a very interesting research challenge. Although a good efficiency has been achieved for these devices using single-crystalline materials such as silicon and compound semiconductors,[1] the manufacturing processes are still relatively expensive in terms of both materials and techniques. On the other hand, organic and dye-sensitized solar cells can be manufactured more inexpensively due to the use of solution-processed materials, making them beneficial. However, further enhancement of the power conversion efficiency (PCE) is still required for practical applications. In addition to the efforts to increase PCE and reduce fabrication cost, long-term operation without the degradation of the active materials must be considered to be an equally important factor.

Recently, methylammonium lead halide ($CH_3NH_3PbX_3$, X = halogen; CH_3NH_3: MA) and its mixed-halide crystals, corresponding to three-dimensional perovskite structures, have been used as light harvesters for solar cells.[2−4] The advantages of these compounds have already been demonstrated as a noteworthy example of potentially useful physical properties such as nonlinear optical properties, electroluminescence, organic-like mobility, magnetic properties, conductivity, and so forth.[5−8] Perovskite-based hybrids can be synthesized using simple and cheap techniques due to their self-assembling character.[8] Thus, these hybrid materials have the potential to be ideal light harvesters for low-cost and high-efficiency solar cells. The cell architectures for solar cells consist of a porous layer of a nanocrystalline metal oxide covered with sunlight-absorbing $MAPbX_3$ and a hole-transporting material. They are cost-effective due to their simple fabrication process and high PCE. As a result, these cells have attracted a great deal of attention among researchers in the field. Furthermore, these inorganic–organic hybrid solar cells may have another distinct advantage: the band gap of $MAPbX_3$ can easily be tuned by chemical management to produce an array of translucent colors, and this feature can be used to create colorful solar designs. As a result, these solar cells may have various building applications, such as in replacing windows, roofs, and even walls. They can be designed to address functional requirements while at the same time producing electricity from the sun.

Band-gap tuning of $MAPbX_3$ has been achieved via substitution of I with Br ions, which arises from a strong dependence of electronic energies on the effective exciton mass.[9] We fabricated inorganic–organic heterojunction solar

Received: January 28, 2013
Revised: March 7, 2013

dx.doi.org/10.1021/nl400349b | *Nano Lett.* XXXX, XXX, XXX–XXX

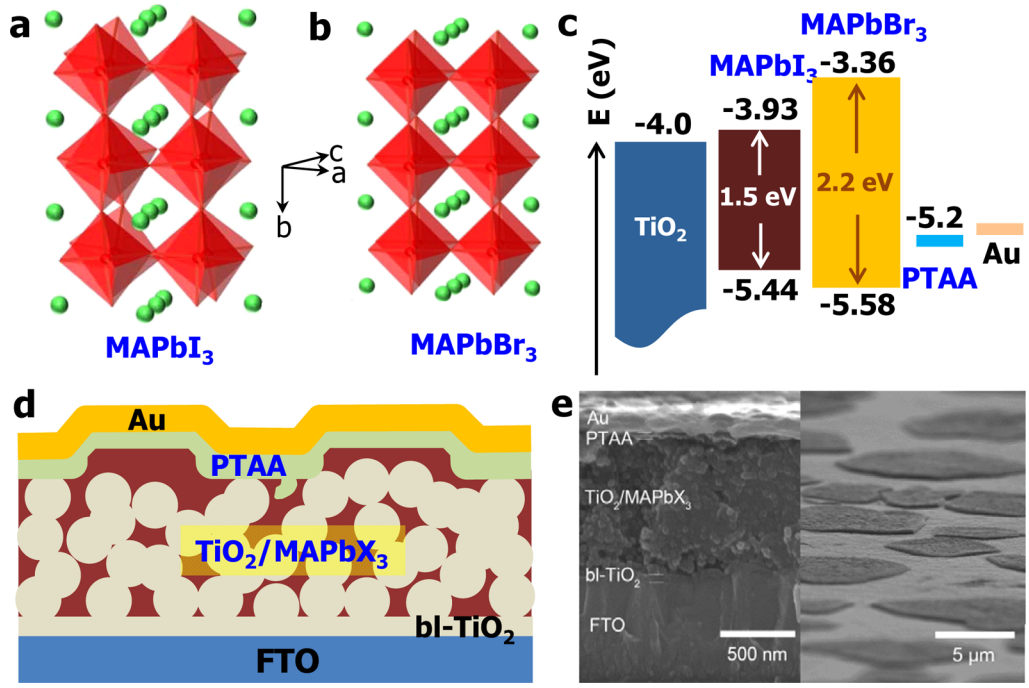

Figure 1. Crystal structures and energy levels of $MAPbI_3$ and $MAPbBr_3$ and hybrid heterojunction solar cell configuration. (a) Distorted tetragonal perovskite structure of $MAPbI_3$ at room temperature. (b) Cubic perovskite structure of $MAPbBr_3$ at room temperature. Red: polyhederon $[PbX_{6/2}]^-$ (X = I, Br); green sphere: CH_3NH_3(= MA). (c) The conduction band minimum (CBM) and the valence band maximum (VBM) of $MAPbI_3$, $MAPbBr_3$, and TiO_2 are represented in eV. (d) Device configuration of the hybrid heterojunction solar cell consisting of the 3D $TiO_2/MAPbX_3$ bilayer nanocomposites, PTAA layer, and Au layer on the blocking TiO_2 layer (bl-TiO_2) coated FTO substrate. (e) FESEM images in cross sectional view (left) and tilted surface view (right) of the real device.

cells by using an entire range of $MAPb(I_{1-x}Br_x)_3$ as light harvesters on mesoporous (mp) TiO_2 and polytriarylamine (PTAA), which act as hole-transporting materials (HTMs). Interestingly, the cells fabricated with $MAPb(I_{1-x}Br_x)_3$ performed stably at $x = 0.2$ compared with other compositions, and the substitution of I with Br also led to improved efficiency with a maximum power conversion efficiency of 12.3% under air-mass 1.5 global (AM 1.5G) illumination of 100 mW cm^{-2} intensity.

$MAPbI_3$ has a distorted three-dimensional perovskite structure that crystallizes in the tetragonal *I*4/*mcm* space group, while $MAPbBr_3$ has a cubic perovskite structure phase of the $Pm\bar{3}m$ space group at room temperature, as shown in Figure 1a and b.[10] The structural difference between the two perovskites seems to originate from the differences in the ionic radius of I^- and Br^- ions with 6-fold coordination, which are 2.2 and 1.96 Å, respectively. The ionic radii relationship of A, M, and X in AMX_3 perovskite structure has been widely accepted as a criterion for the distortion of the MX_6 octahedron; that is, the formation or stability of cubic perovskite structure and the smaller X ion radius is relatively profitable for the formation of cubic structure.[8,11] The band gaps of $MAPbI_3$ and $MAPbBr_3$ were reported as 1.5 and 2.3 eV, respectively.[3,4,12] As can be seen by the band alignment (Figure 1c), these two materials have a suitable band position for heterojunction solar cells using a mesoscopic TiO_2 photoelectrode since the conduction band energy (CBE) of both $MAPbI_3$ and $MAPbBr_3$ is higher than that for TiO_2. Here we expect that band gap-tailored light harvesters can be simply designed by the alloying of $MAPbI_3$ and $MAPbBr_3$. Figure 1d shows the schematic device architecture of hybrid heterojunction solar cell with a pillared $MAPbX_3$ overlayer. Upon illumination of light, the $MAPbX_3$ perovskite absorbs the light and generates electron−hole pairs. The electrons are injected into TiO_2, and simultaneously the hole is transported to PTAA and/or counter electrode through the perovskite itself.[13,14] The cross-sectional and tilted SEM image in Figure 1e confirms that the cell configuration is a three-dimensional bilayer structure with a pillared $MAPbX_3$ overlayer. In our previous work,[13] we reported that the $MAPbX_3$ is densely infiltrated into the pores of mp-TiO_2 layer and interconnected with overlayer. PTAA was mostly located on and near the surface of the pillared structure.

Figure 2a exhibits X-ray diffraction (XRD) patterns monitored in the 2θ range of 27.5−31° for $MAPb(I_{1-x}Br_x)_3$ ($0 \le x \le 1$) with increasing Br ions. The XRD patterns of $MAPbI_3$ and $MAPbBr_3$ in Supplemental Figure S1 indicate that $MAPbI_3$ and $MAPbBr_3$ have tetragonal and cubic perovskite phases at room temperature, respectively, that are in agreement with the reported structures.[10] The $MAPbI_3$ ($x = 0$) has two peaks located at 28.11° and 28.36° which can be indexed to the (004) and (220) planes for the tetragonal *I*4/*mcm* phase.[4] The peak diffracted by the (004) plane gradually disappears upon increasing x and finally merges into a single peak corresponding to (200) around $x = 0.2$ due to the increased symmetry. In other words, the tetragonal phase of $MAPbI_3$ is maintained until $x = 0.13$ and then transits to a cubic phase around $x = 0.2$. Because the *I*4/*mcm* phase is transited from the $Pm\bar{3}m$ phase in the ideal $MAPbX_3$ perovskite structure by the slight rotation of the PbX_6 octahedrons along the ⟨001⟩ axis on the (00*l*) plane while maintaining their corner-sharing connectivity, the tetragonal phase can be defined by a pseudocubic (pc) lattice, as shown in Figure 2b. Therefore, the $(100)_{pc}$ spacing in a pseudocubic crystal system can match the $(110)_t$ spacing in a tetragonal (t) crystal system in the $MAPb(I_{1-x}Br_x)_3$ phase. The

dx.doi.org/10.1021/nl400349b | *Nano Lett.* XXXX, XXX, XXX−XXX

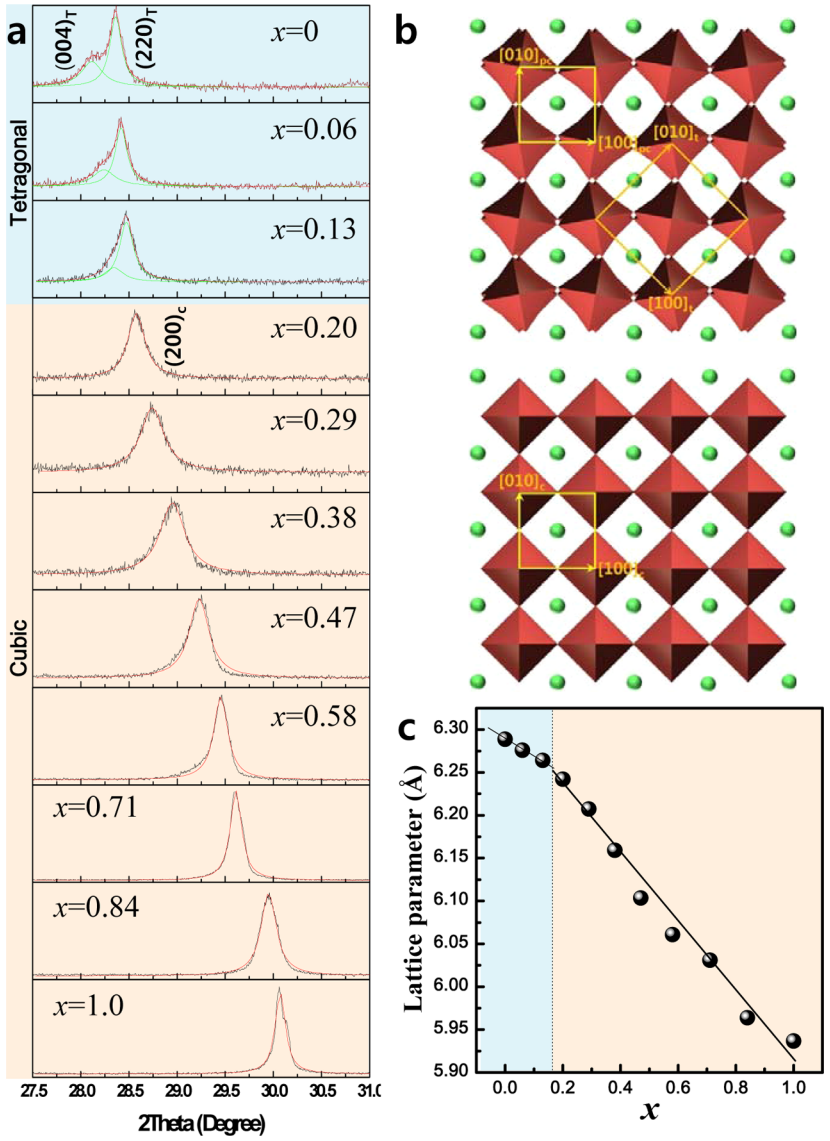

Figure 2. X-ray diffraction analysis of the $MAPb(I_{1-x}Br_x)_3$. (a) XRD patterns of $MAPb(I_{1-x}Br_x)_3$ (x = 0, 0.06, 0.13, 0.20, 0.29, 0.38, 0.47, 0.58, 0.71, 0.84, 1.0), magnified in the region of the tetragonal $(004)_T$ and $(220)_T$ and cubic $(200)_C$ peaks (2θ = 27.5−31.0°). (b) Crystal structures and unit lattice vectors on the (00l) plane of the tetragonal ($I4/mcm$) (top) and cubic ($Pm\bar{3}m$) (bottom) phases are represented. The tetragonal lattice can be taken by the pseudocubic (pc) lattice. (c) Lattice parameters of pseudocubic or cubic $MAPb(I_{1-x}Br_x)_3$ as a function of Br composition (x).

further introduction of Br ions into $MAPbI_3$ instead of I ions causes the systematic shift of the $(200)_c$ peak toward higher 2θ degrees because the gradual substitution of the larger I atoms with the smaller Br atoms decreases the lattice spacing. Figure 2c exhibits the lattice parameter a of the $MAPb(I_{1-x}Br_x)_3$ phases indexed by pseudocubic or cubic as a function of Br content (x). Although the slope is slightly changed at the tetragonal to cubic phase transition point between x = 0.13 and 0.20, the lattice parameter of $MAPb(I_{1-x}Br_x)_3$ ($0 \le x \le 1$) phases exhibits a linear relationship with the Br content in each region. According to Vegard's law, the variation of the lattice parameter in the alloy is linear with composition in the absence of strong electronic effects.[15,16] Therefore, the linear trend indicates the formation of the $MAPb(I_{1-x}Br_x)_3$ compound in the entire range of $MAPb(I_{1-x}Br_x)_3$ ($0 \le x \le 1$) by a simple solution-mixing process.

To check the variation of optical properties in the alloyed hybrid perovskite, we measured the UV−visible absorption spectra of mp-TiO_2/$MAPb(I_{1-x}Br_x)_3$ ($0 \le x \le 1$), as shown in Figure 3a. The onset absorption band of $MAPb(I_{1-x}Br_x)_3$ nanocomposites can be tuned from a 786 nm wavelength (1.58 eV) to 544 nm wavelength (2.28 eV), resulting in color tunability for colorful solar cells. Figure 3b shows the corresponding device colors of mp-TiO_2/$MAPb(I_{1-x}Br_x)_3$ ($0 \le x \le 1$). Through the compositional control of $MAPb(I_{1-x}Br_x)_3$, we could tune the color from dark brown for mp-TiO_2/$MAPbI_3$ (x = 0) to brown/red for mp-TiO_2/$MAPb(I_{1-x}Br_x)_3$ and then to yellow for mp-TiO_2/$MAPbBr_3$ (x = 1) with increasing Br content. A systematic shift of the absorption band edge to shorter wavelength with increasing Br content in $MAPb(I_{1-x}Br_x)_3$ ($0 \le x \le 1$) indicates that the energy band gap (E_g) can be tuned by the composition of the alloy. The E_g (estimated from the onset absorption band) variation with the Br content in $MAPb(I_{1-x}Br_x)_3$ was plotted in Figure 3c. Empirically, the nonlinear variation of E_g with a composition in the alloy can be expressed by following quadratic eq 1:

dx.doi.org/10.1021/nl400349b | Nano Lett. XXXX, XXX, XXX−XXX

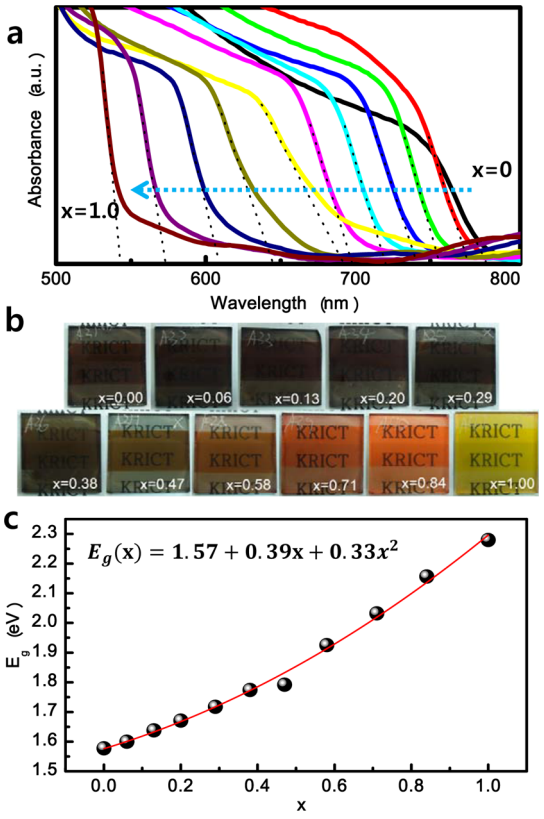

Figure 3. Photographs and UV−vis absorption spectra of MAPb$(I_{1-x}Br_x)_3$. (a) UV−vis absorption spectra of FTO/bl-TiO_2/mp-TiO_2/MAPb$(I_{1-x}Br_x)_3$/Au cells measured using an integral sphere. (b) Photographs of 3D TiO_2/MAPb$(I_{1-x}Br_x)_3$ bilayer nanocomposites on FTO glass substrates. (c) A quadratic relationship of the band-gaps of MAPb$(I_{1-x}Br_x)_3$ as a function of Br composition (x).

$$E_g[\mathrm{MAPb}(I_{1-x}Br_x)_3] = E_g[\mathrm{MAPbI_3}] + (E_g[\mathrm{MAPbBr_3}] - E_g[\mathrm{MAPbI_3}] - b)x + bx^2 \quad (1)$$

where b is the bowing parameter.[17,18] A least-squares fit (red line) of E_g in Figure 3c changes the eq 1 to eq 2 which yields the bowing parameter of b = 0.33 eV.

$$E_g(x) = 1.57 + 0.39x + 0.33x^2 \quad (2)$$

The extent of bowing is a measure of the degree of fluctuations in the crystal field or the nonlinear effect arising from the anisotropic nature of binding.[19] The quite small bowing parameter (b = 0.33 eV) in MAPb$(I_{1-x}Br_x)_3$ compared with those of other alloys indicates that $MAPbI_3$ and $MAPbBr_3$ have a great miscibility.[19,20] This confirms again that MAPb$(I_{1-x}Br_x)_3$ makes up the entire composition of the compound and consequently enables convenient band gap tailoring by a simple mixing process.

Figure 4a and b shows the trend of PCE as a function of x in the cells fabricated with MAPb$(I_{1-x}Br_x)_3$ and the J−V characteristics at x = 0, 0.06, 0.13, 0.20, 0.29, 0.58, and 1.0, respectively. The current density (J_{sc}) is decreased from 18 mA cm^{-2} at x = 0 to 5 mA cm^{-2} at x = 1 with increasing x, whereas open circuit voltage (V_{oc}) is increased from 0.87 to 1.13 V. In addition to the significant improvement in V_{oc}, an increase in the fill factor (FF) from 0.66 to 0.74 was also observed upon

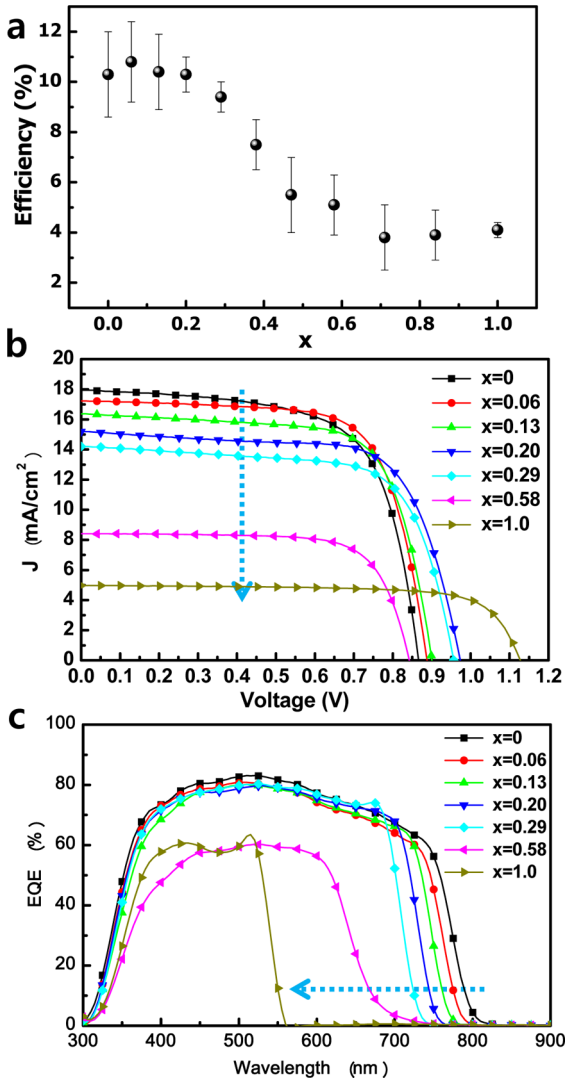

Figure 4. Photovoltaic characteristics of the MAPb$(I_{1-x}Br_x)_3$ heterojunction solar cells. (a) Power conversion efficiencies of the heterojunction solar cells as a function of Br composition (x). (b) Photocurrent density−voltage (J−V) characteristics of the heterojunction solar cells based on MAPb$(I_{1-x}Br_x)_3$ (x = 0, 0.06, 0.13, 0.20, 0.29, 0.58, 1.0). (c) Corresponding external quantum efficiency (EQE) spectra.

the incorporation of the Br ions. It is well-known that the series resistance (R_s) greatly affects the fill factor and efficiency of solar cells. The main contribution to R_s comes from (1) the active and interfacial layer resistances, (2) electrode resistances, and (3) the base contact resistances.[21] In our work, R_s among the cells fabricated from MAPb$(I_{1-x}Br_x)_3$ will be mainly caused by the difference of (1) the active layer resistance as light harvester, because factors (2) and (3) will be similar due to the use of same architecture and materials in the cell configuration. Based on these facts, we compared the slope obtained from the relationship between reciprocal series resistance and short circuit current density (J_{sc}) for undoped $MAPbI_3$ and Br-doped MAPb$(I_{0.9}Br_{0.1})_3$ as light harvesters. As can be seen in Figure S3, Br-doped cell has steeper slope than undoped cell, suggesting that the charge transport properties are substantially improved.

The reduction of J_{sc} with increasing x is directly related with the blue-shift of absorption onset, which is responsible for the

dx.doi.org/10.1021/nl400349b | Nano Lett. XXXX, XXX, XXX−XXX

increased band gap, as explained previously. The improvement of V_{oc} is attributed to the widening of the band gap with increasing x in MAPb$(I_{1-x}Br_x)_3$. Therefore, the PCE of the solar cells fabricated with MAPb$(I_{1-x}Br_x)_3$ in the range from x = 0 to 0.20 might exhibit similar average values over 10% at a light illumination of 100 mW cm^{-2} AM 1.5 G due to the simultaneous enhancement of V_{oc} and FF against J_{sc} decreased by adding Br ions because PCE is determined from the products of J_{sc}, V_{oc}, and FF (Figure 4a). Nevertheless, an abrupt reduction of V_{oc} between x = 0.20 and x = 0.58 in MAPb$(I_{1-x}Br_x)_3$ was observed. This means that there are additional factors influencing the cell performance of MAPb$(I_{1-x}Br_x)_3$ with increasing x except the band gap. We surmise that charge transport and recombination behavior of MAPb$(I_{1-x}Br_x)_3$ acting as both light harvester and hole transport was greatly changed near of x = 0.58 in MAPb$(I_{1-x}Br_x)_3$, even though the MAPb$(I_{1-x}Br_x)_3$ compound uniformly formed in the entire range. The external quantum efficiency (EQE) spectra of the devices illuminated by monochromatic light are shown in Figure 4c. An average EQE approaching 80% in the range of 450−600 nm was observed for the cells fabricated with x = 0, 0.06, 0.13, 0.20, 0.29 in MAPb$(I_{1-x}Br_x)_3$, and the integrated photocurrent density from EQE spectra were also well matched with the J_{sc}.

It was known that perovskite-type hybrids are easily decomposed in the presence of moisture because of the hygroscopic amine salts. This restricts the use of halide compounds for many practical applications. In particular, $MAPbI_3$ is more sensitive to moisture compared with $MAPbBr_3$.[8] To investigate the stability of MAPb$(I_{1-x}Br_x)_3$ hybrid solar cells with the composition, we measured the PCE of the unencapsulated MAPb$(I_{1-x}Br_x)_3$ (x = 0, 0.06, 0.20, and 0.29 as representative model device) hybrid solar cells under ambient conditions with controlled humidity along with the storage time, as shown in Figure 5. Although the $MAPbI_3$ hybrid solar cell does not exhibit significant degradation of PCE at low humidity (<50%), we found that $MAPbI_3$ began to decompose at relatively high humidity (≥55%), displaying a color change from dark brown to yellow. Hence, we intentionally exposed the solar cells to relatively high humidity (55%) for one day while keeping the humidity to 35% on the other days. Interestingly, the MAPb$(I_{1-x}Br_x)_3$ (x = 0, 0.06) hybrid solar cells exhibited serious degradation of PCE after exposure to 55% humidity, whereas the other MAPb$(I_{1-x}Br_x)_3$ (x = 0.2, 0.29) cells maintained the PCE. A low sensitivity to the humidity of the cells based on MAPb$(I_{1-x}Br_x)_3$ ($x \geq 0.2$) might be associated with its compact and stable structure, because the substitution of larger I atoms with smaller Br atoms in MAPb$(I_{1-x}Br_x)_3$ leads to the reduction of the lattice constant and a transition to a cubic phase, as shown Figure 2c. The XRD patterns of the MAPb$(I_{1-x}Br_x)_3$ (x = 0, 0.06, 0.20) device after 20 days of stability testing confirmed that cubic phase MAPb$(I_{1-x}Br_x)_3$ ($x \geq 0.2$) cells have better stability than tetragonal (pseudocubic) phase MAPb$(I_{1-x}Br_x)_3$ ($x < 0.2$) cells. This is evident because the MAPb$(I_{1-x}Br_x)_3$ (x = 0, 0.06) cells exhibited an additional PbI_2 peak after decomposition, which can be measured by the color change from dark brown to yellow, whereas the MAPb$(I_{1-x}Br_x)_3$ ($x \geq 0.2$) cells did not exhibit any additional peaks (see Supplemental Figure S2). These results indicate that it is possible to greatly improve the stability of the cells fabricated from perovskite $MAPbX_3$ families by controlling the composition without damaging the cell performance.

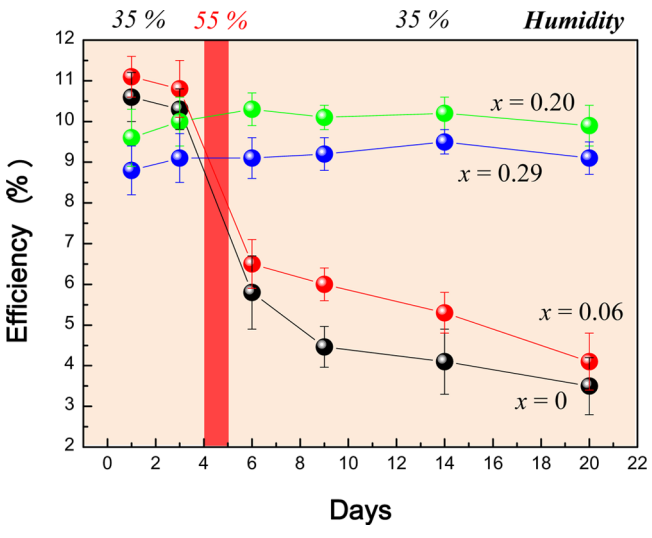

Figure 5. Power conversion efficiency variation of the heterojunction solar cells based on MAPb$(I_{1-x}Br_x)_3$ (x = 0, 0.06, 0.20, 0.29) with time stored in air at room temperature without encapsulation. The humidity was maintained at 35%, and the cells were exposed to a humidity of 55% for one day on the fourth day to investigate performance variation at high humidity.

In summary, we have demonstrated enhanced power conversion efficiency and stability through the chemical management of $MAPbX_3$ (X = halogen) with the possible fabrication of colorful solar cells due to the tunable band gap. The lattice parameters and successive band gap energy (E_g) of MAPb$(I_{1-x}Br_x)_3$ were found to have linear relationships with Br content (x). The optical absorption caused by band gap engineering can be controllably tuned to cover almost the entire visible spectrum. The cells fabricated from x = 0 to 0.2 in MAPb$(I_{1-x}Br_x)_3$ exhibit an average of more than 10% with maximum 12.3% in conversion efficiency under full sun (100 mW cm^{-2}) of AM 1.5 G radiation, and at x = 0.2, the relative stability under same conditions was greatly improved while keeping the efficiency. Therefore, the present findings will be one of noble approaches for future practical applications with excellent perspectives.

■ ASSOCIATED CONTENT

Ⓢ Supporting Information

Details of experiments and additional supplementary figures. This material is available free of charge via the Internet at http://pubs.acs.org.

■ AUTHOR INFORMATION

Corresponding Author

*E-mail: seoksi@krict.re.kr (seoksi@skku.edu).

Author Contributions

J.H.N., S.H.I., and J.H.H. contributed equally to this work.

Notes

The authors declare no competing financial interest.

■ ACKNOWLEDGMENTS

This study was supported by the Global Research Laboratory (GRL) Program and the Global Frontier R&D Program on Center for Multiscale Energy System funded by the National Research Foundation under the Ministry of Education, Science

and Technology of Korea, and by a grant from the KRICT 2020 Program for Future Technology of the Korea Research Institute of Chemical Technology (KRICT), Republic of Korea.

REFERENCES

(1) Green, M. A.; Emery, K.; Hishikawa, Y.; Warta, W.; Dunlop, E. D. *Prog. Photovolt.: Res. Appl.* **2012**, *20*, 12−20.
(2) Lee, M. M.; Teuscher, J.; Miyasaka, T.; Murakami, T. N.; Snaith, H. J. *Science* **2012**, *338*, 643−647.
(3) Kim, H.-S.; Lee, C.-R.; Im, J.-H.; Lee, K.-B.; Moehl, T.; Marchioro, A.; Moon, S.-J.; Humphry-Baker, R.; Yum, J.-H.; Moser, J. E.; Grätzel, M.; Park, N.-G. *Sci. Rep.* **2012**, *2*, 591:1−7.
(4) Kojima, A.; Teshima, K.; Shirai, Y.; Miyasaka, T. *J. Am. Chem. Soc.* **2009**, *131*, 6050−6051.
(5) Koutselas, I.; Bampoulis, P.; Maratou, E.; Evagelinou, T.; Pagona, G.; Papavassiliou, G. C. *J. Phys. Chem. C* **2011**, *115*, 8475−8483.
(6) Li, C. R.; Deng, H. T.; Wan, J.; Zheng, Y. Y.; Dong, W. J. *Mater. Lett.* **2010**, *64*, 2735−2737.
(7) Patrin, G. S.; Volkov, N. V.; Prokhorova, I. V. *Phys. Solid State* **2004**, *46*, 1891−1894.
(8) Cheng, Z.; Lin, J. *CrystEngComm* **2010**, *12*, 2646−2662.
(9) Tanaka, K.; Takahashi, T.; Ban, T.; Kondo, T.; Uchida, K.; Miura, N. *Solid State Commun.* **2003**, *127*, 619−623.
(10) Poglitsch, A.; Weber, D. *J. Chem. Phys.* **1987**, *87*, 6373−6378.
(11) Galasso, F. S. *Structure, Properties and Preparation of Perovskite-type Compounds*; Pergamon: New York, 1969.
(12) Kitazawa, N.; Watanabe, Y.; Nakamura, Y. *J. Mater. Sci.* **2002**, *37*, 3583−3587.
(13) Heo, J. H.; Im, S. H.; Noh, J. H.; Mandal, T. N.; Lim, C.-S.; Chang, J. A.; Lee, Y. H.; Kim, H.; Sarkar, A.; Nazeeruddin, M. K.; Grätzel, M.; Seok, S. I. *Nat. Photonics*, in press.
(14) Etgar, L.; Gao, P.; Xue, Z.; Peng, Q.; Chandiran, A. K.; Liu, B.; M., K.; Grätzel, M. *J. Am. Chem. Soc.* **2012**, *134*, 17396−17399.
(15) Vegard, L. *Z. Phys.* **1921**, *5*, 17−26.
(16) Xu, J.; Tang, Y.-B.; Chen, X.; Luan, C.-Y.; Zhang, W.-F.; Zapien, J. A.; Zhang, W.-J.; Kwong, H.-L.; Meng, X.-M.; Lee, S.-T.; Lee, C.-S. *Adv. Funct. Mater.* **2010**, *20*, 4190−4195.
(17) El-Shazly, A. A.; El-Naby, M. M. H.; Kenawy, M. A.; El-Nahass, M. M.; El-Shair, H. T.; Ebrahim, A. M. *Appl. Phys. A: Mater. Sci. Process.* **1985**, *36*, 51−53.
(18) Wang, M.; Fei, G. T.; Zhang, Y. G.; Kong, M. G.; Zhang, L. D. *Adv. Mater.* **2007**, *19*, 4491−4494.
(19) Hill, R. *J. Phys. C: Solid State Phys.* **1974**, *7*, 521−526.
(20) Venugopal, R.; Lin, P.-I.; Chen, Y.-T. *J. Phys. Chem. B* **2006**, *110*, 11691−11696.
(21) Servaites, J. D.; Yeganeh, S.; Marks, T. J.; Ratner, M. A. *Adv. Funct. Mater.* **2010**, *20*, 97−104.